

Transfer Free Energies and Partitioning of Small Molecules in Collapsed PNIPAM Polymers

Matej Kanduč,^{1,2,*} Won Kyu Kim,¹ Rafael Roa,³ and Joachim Dzubiella^{4,1,†}

¹Research Group for Simulations of Energy Materials,
Helmholtz-Zentrum Berlin für Materialien und Energie,
Hahn-Meitner-Platz 1, D-14109 Berlin, Germany

²Jožef Stefan Institute, Jamova 39, SI-1001 Ljubljana, Slovenia

³Departamento de Física Aplicada I, Facultad de Ciencias,
Universidad de Málaga, Campus de Teatinos s/n, E-29071 Málaga, Spain

⁴Applied Theoretical Physics – Computational Physics,
Physikalisches Institut, Albert-Ludwigs-Universität Freiburg,
Hermann-Herder Strasse 3, D-79104 Freiburg, Germany

A central quantity in the design of functional hydrogels used as nanocarrier systems, for instance for drug delivery or adaptive nanocatalysis, is the partition ratio, which quantifies the uptake of a molecular substance by the polymer matrix. By employing all-atom molecular dynamics simulations, we study the solvation and partitioning (with respect to bulk water) of small subnanometer-sized solutes in a dense matrix of collapsed Poly(N-isopropylacrylamide) (PNIPAM) polymers above the lower critical solution temperature (LCST) in aqueous solution. We examine the roles of the solute's polarity and its size on the solubility properties in the thermoresponsive polymer. We show that the transfer free energies of nonpolar solutes from bulk water into the polymer are favorable and scale in a good approximation with the solute's surface area. Even for small solute size variation, partitioning can vary over orders of magnitude. A polar nature of the solute, on the other hand, generally opposes the transfer, at least for alkyl solutes. Finally, we find a strong correlation between the transfer free energies in the gel and the adsorption free energies on a single extended polymer chain, which enables us to relate the partition ratios in the swollen and collapsed state of a PNIPAM gel.

I. INTRODUCTION

Stimuli-responsive hydrogels are one of the most promising types of polymers in the development of new soft functional materials [1]. Their attractiveness stems mainly from their responsive nature, tunable water content, and rubbery character, as they resemble the features of biological tissue [2]. These properties made them a key ingredient in many applications in material science, especially as nanocarrier systems, spanning from drug delivery [2–6], catalysis [7–9], biosensing [6, 10], thin-film techniques [6], as well as in environmental science [11], including nanofiltration and water purification [12–14]. Undoubtedly, the most studied thermoresponsive polymer is poly(N-isopropylacrylamide) (PNIPAM), which exhibits the volume transition in water close to the human body temperature [15–17]. As a versatile model component, it has served as a prototype for many developments of soft responsive materials [3, 18, 19].

Clearly, the complete description of a hydrogel material requires the knowledge of many material parameters. Yet, the quantity of central importance is the partition ratio K , defined as the ratio of the concentration of the molecular compound in the hydrogel relative to that in water in thermodynamic equilibrium [20, 21]. The partition ratio is used to assess the transfer processes, the uptake of a compound by the hydrogel, the permeability of a compound, and its fate in a hydrogel-based nanocarrier [22, 23]. Unfortunately, accurate experimental measurements of partition ratios present a serious challenge for many materials [22].

Predictions of the partitioning in collapsed hydrogels are notoriously difficult, owing to the crowded environment with complex polymer–water interactions [24]. Partition ratios are many times greater than predicted by size-exclusion theories, which assume simple steric hindrance of solutes by the network. In fact, because of a lower water content, a collapsed hydrogel exhibits a more hydrophobic environment than in the swollen state, therefore the partition ratio of many hydrophobic compounds (typically drugs) can exceed unity (that is, bulk concentration) by orders of magnitude [25–27].

Thus, estimations of partition ratios rely, especially

* matej.kanduc@ijs.si

† joachim.dzubiella@physik.uni-freiburg.de

in pharmaceutical research, on various heuristic approaches that are based on statistical analysis of big experimental data collections [28–30]. They typically involve different descriptors, such as the size of the molecule, hydrogen-bond counts, the Coulomb energy, etc. [29, 30] However, the large numbers of descriptors that are featured in heuristic models and neural networks obscure the physical basis of solvation [29]. Alternatively, for a basic understanding of the solvation and partitioning processes, one needs to resort to various computer modeling techniques. They typically comprise multiscale approaches, spanning from coarse-grained implicit-solvent models [31–36] to all-atom models [37–40]. Our broader research goal lies in a qualitative molecular-level understanding of thermodynamic and transport properties in PNIPAM-based hydrogels. Employing atomistic, explicit-water simulations, we studied solute partitioning in swollen gels [40] and diffusion inside collapsed gels [41].

In this study, we adopt the previous models to investigate the solvation and partitioning in collapsed PNIPAM polymers of several polar and nonpolar molecules, featuring small alkanes, simple alcohols, and aromatic molecules.

II. METHODS

Atomistic model. We set up an atomistic model of collapsed PNIPAM polymer chains in explicit water. The collapsed polymer can also serve as an approximate model for a collapsed hydrogel with very low (few percents) cross-linker concentrations. We utilize the same simulation model as in our recent work [41], which primarily focuses on molecular diffusion. To briefly recap, the PNIPAM chains are composed of 20 monomeric units with atactic stereochemistry (*i.e.*, with random distribution of monomeric enantiomers along the chain). For PNIPAM polymers we adopt the recent OPLS-based force field by Palivec et al. [42] with an *ad hoc* parametrization of partial charges, which reproduces the thermoresponsive properties much better than the standard OPLS-AA force field, even though the latter one used to be very popular for PNIPAM simulations [37, 43–48]. For water we use the SPC/E water model [49], and the OPLS-AA force field [50, 51] for solute molecules. This force field combination keeps our model on a generic level and captures the hydration properties of solutes in water very well [52], as we also demonstrate in *Supporting Information*.

Equilibrated molecular structures of the collapsed PNIPAM polymers with water were taken from the previous study [41]. First, 48 polymer chains were solvated in excess water above the transition temperature (≈ 305 K), which caused the polymers to phase separate from the water phase. The amount of water in the polymer precipitate was then used as an input parameter to construct a simulation setup that mimics a bulk of collapsed PNIPAM (Figure 1a) with employed periodic boundary conditions in all three directions. The amount of water (Figure 1b) in the PNIPAM thus corresponds to the equilibrium amount with an external bulk water reservoir, which depends on temperature, as shown in Figure 1c.

Simulation details. The molecular dynamics (MD) simulations were carried out with the GROMACS 5.1 simulation package [56, 57] in the constant-pressure (NPT) ensemble, where the box sizes are independently adjusted in order to maintain the external pressure of 1 bar via the Berendsen barostat [58] with the time constant of 1 ps. The system temperature was maintained by the velocity-rescaling thermostat [59] with the time constant of 0.1 ps. The Lennard-Jones (LJ) interactions were truncated at 1.0 nm. Electrostatics was treated using Particle-Mesh-Ewald (PME) methods [60, 61] with the real-space cutoff of 1.0 nm.

A. Solvation free energies. In order to perform free energy calculations of the solutes (Figure 2), we first insert 10–15 solute molecules of the same kind at random positions in an equilibrated system of PNIPAM polymers and water. The system (with fully interacting solutes) then undergoes further equilibration, where the necessary equilibration times of the solutes are estimated based on the crossover times of the solutes to reach the normal diffusion [41] (such that a solute performs at least a few hopping events and reaches its equilibrium hydration). The equilibration times thus span from several 100 ps for the smallest solutes (He and Ne) and up to several 100 ns for the largest (NP^0).

The solvation free energies of the solutes are then computed using the Thermodynamic Integration (TI) technique [62], with the strength of the interaction potential of the solutes as the thermodynamic path. Within this procedure, the solute’s partial charges and all LJ interactions between the solute molecule and other molecules are gradually switched off. Introducing a coupling parameter $\lambda \in [0, 1]$ that continuously switches the interactions in

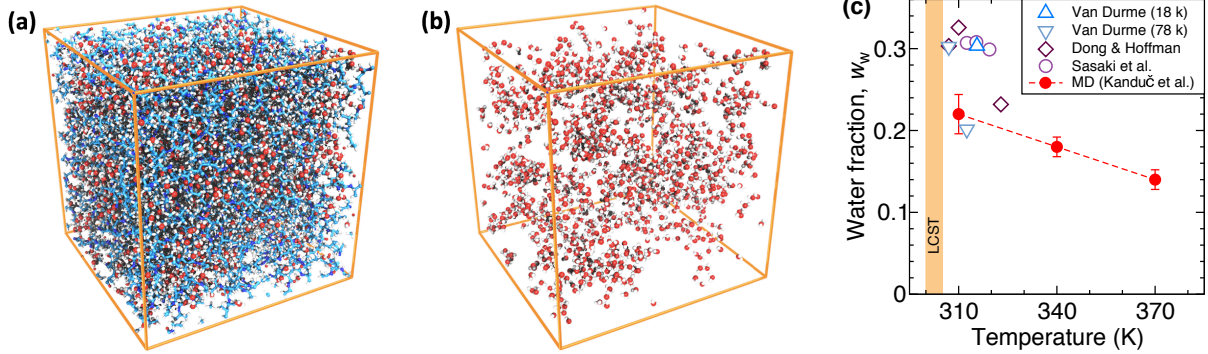


FIG. 1. Snapshots of collapsed PNIPAM at 340 K showing (a) all atoms and (b) only water molecules. (c) Mass fraction of water in the collapsed PNIPAM that corresponds to chemical equilibrium with bulk water as determined in our previous study [41] (red circles). Open symbols show different experimental measurements: Triangles are the PNIPAM/water coexistence (binodal) curves by Van Durme et al. [53] for molecular weights of 18 and 78 kDa. Diamonds and circles represent the water amount in PNIPAM hydrogels (*i.e.*, cross-linked networks) by Dong and Hoffman [54] and Sasaki et al. [55], respectively.

the Hamiltonian $U(\lambda)$ between the original solute interactions (for $\lambda = 1$) and a non-interacting particle (for $\lambda = 0$), the solvation free energy is computed as [62]

$$G^{\text{TI}} = \int_0^1 \left\langle \frac{\partial U(\lambda)}{\partial \lambda} \right\rangle_\lambda d\lambda \quad (1)$$

The integration is performed in two stages: We first linearly scale down the partial charges of the solute particle, while keeping the LJ interactions intact. In the second stage, we scale the LJ interactions using the “soft-core” LJ functions as implemented in GROMACS [56, 57] in order to circumvent singularities when the potentials are about to vanish ($\lambda \rightarrow 0$) [63]. We separate the entire TI procedure into 24 individual simulations with equidistant λ values for the Coulomb part and likewise 24 simulations for the LJ part. The simulation time of each individual simulation with given λ is 4 ns where the first 0.1–3 ns are discarded from sampling to allow equilibration of the solutes. The estimation of the equilibration time in each individual simulation is based on the drift of the $(\partial U/\partial \lambda)$ output. All the TI calculations are performed using 2–5 independently equilibrated systems. The final results are averaged over all the particles in a simulation box and over all the systems. Even though each particle samples only a local phase space during a short TI time window, such an averaging assures adequately sampled values of the free energy. We have also verified that solute–solute interactions during TI have negligible effects on the free energy evaluation (see *Supporting Information*).

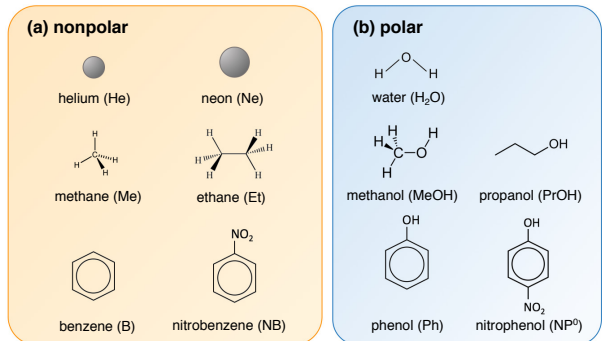


FIG. 2. Solute molecules in our study: (a) nonpolar molecules and (b) polar molecules (characterized by the hydroxyl group).

The solvation free energies for transferring a solute from the vacuum (or the gas phase) into the medium (*i.e.*, bulk water or PNIPAM; $i = w, p$, respectively) are obtained by subtracting the free energy value (eq 1) obtained from TI in vacuum from the value in the medium, $G_i = G_{(\text{in medium } i)}^{\text{TI}} - G_{(\text{in vacuum})}^{\text{TI}}$. Note that $G_{(\text{in vacuum})}^{\text{TI}}$ may be nonzero due to intra-molecular Coulombic and LJ contributions.

B. Molecular surface area. A convenient and simple way to characterize the effective size of a solute is based on its surface area. For our purposes, we consider a solute as a union of fused

van der Waals spheres. The *molecular surface area*, A_m , is then the envelope area of the fused union of the spheres [64]. This definition is analogous to the concept of the solvent accessible surface area (SASA) [65, 66] with vanishing probe radius, $r_0 = 0$, and in a sense corresponds to the surface area of a ‘bare’ solute.

III. RESULTS AND DISCUSSION

A. Water structure in the collapsed polymer. For convenience of the reader we first briefly recall some basic characteristics of the collapsed PNIPAM polymer with sorbed water, as in detail presented in our previous study [41]. We performed simulations at 310, 340, and 370 K (range where PNIPAM is collapsed). Most of our analysis and discussion will be centered around the results at the midpoint temperature of 340 K.

A typical simulation snapshot at 340 K is shown in Figure 1a with PNIPAM chains in blue and water molecules in red–white. For better illustration, the water component of this structure is displayed alone in Figure 1b. Water molecules are far from being uniformly distributed in the polymer phase, but rather structure into nanosized ‘lacy-like’ clusters and pockets. Additionally, the water clusters do not have a characteristic size but are extremely polydisperse, with a size distribution that roughly follows the power law $P(N_w) \propto N_w^{-1.74}$, where N_w is the number of water molecules in the cluster. The radius of gyration R_g of the clusters scales with the size N_w as $R_g \sim N_w^{1/2}$, which is also a characteristic of the random walk [41].

The amount of water varies with temperature such that it always matches the chemical equilibrium with a hypothetical external water reservoir. The corresponding amount has been determined in the previous study [41], and is shown in Figure 1c in terms of mass water fraction, w_w , at different temperatures. The mass fraction of water is the ratio between the water mass density inside PNIPAM, $\rho_w^{(in)}$, and the density of the entire PNIPAM phase, $w_w = \rho_w^{(in)} / \rho_{tot}^{(in)}$. The water fraction linearly decreases with rising temperature, which reflects the increasing hydrophobic character of PNIPAM upon heating. Analogously to the classical partition ratio, we can define the water partition ratio K_w as the density ratio of water inside and outside the polymer. Since the density of the PNIPAM phase is roughly the same as the density of bulk water,

$\rho_{tot}^{(in)} \approx \rho_w^0$ [41], it follows that the water partition ratio approximately equals the water mass fraction,

$$K_w = \frac{\rho_w^{(in)}}{\rho_w^0} \approx w_w \quad (2)$$

B. Distribution of solutes in the PNIPAM phase. Due to the aforementioned water–polymer spatial heterogeneity, one can anticipate that solutes are not going to redistribute uniformly throughout the PNIPAM phase, but will be subject to the water–polymer spatial pattern, whereby the nature of the solute (polar vs. nonpolar) plays a decisive role. For a qualitative appraisal, we show typical snapshots of several solutes in the PNIPAM phase in Figure 3a. As seen, hydroxyl groups tend to stick to water clusters more willingly than their hydrophobic residues.

In order to examine the nature of the solute distribution quantitatively, we probe the local physical environment into which the solutes settle. For that purpose, we define the hydration number n_w as the number of water molecules residing within a spherical shell of radius $r_c = 0.54$ nm (corresponding to the first hydration shell of CH_4 in pure water [41]) around any of the solute’s atoms. In Figure 3b we show the relative hydration of the solutes, defined as the ratio of the hydration numbers inside PNIPAM and in bulk water, $n_w^{(in)} / n_w^{(out)}$. A hypothetical solute that would partition uniformly throughout the PNIPAM phase would feature the relative hydration equal to the water partition ratio, $K_w = 0.19$ (denoted by a dashed line). Not surprisingly, nonpolar solutes get significantly more dehydrated when entering the PNIPAM phase, with relative hydration of only 0.11–0.16 relative to water environment. This means, the nonpolar solutes reside preferentially in ‘dry’ regions of the polymer and are expelled from water clusters. On the contrary, the polar molecules feature on average higher hydration due to the high affinity of the hydroxyl group to water. Clearly, their polar character is diminishing with the size of the nonpolar residue. Thus, polar molecules with larger nonpolar residues (PrOH, Ph, and NP⁰) behave as being nonpolar in that sense, with the relative hydration below K_w .

C. Solvation free energies. We now turn to the solvation free energies, as they are central quantities for resolving the partition ratios of the solutes. The solvation free energies for the transfer of a solute from vacuum (or ideal gas phase) into water (G_w)

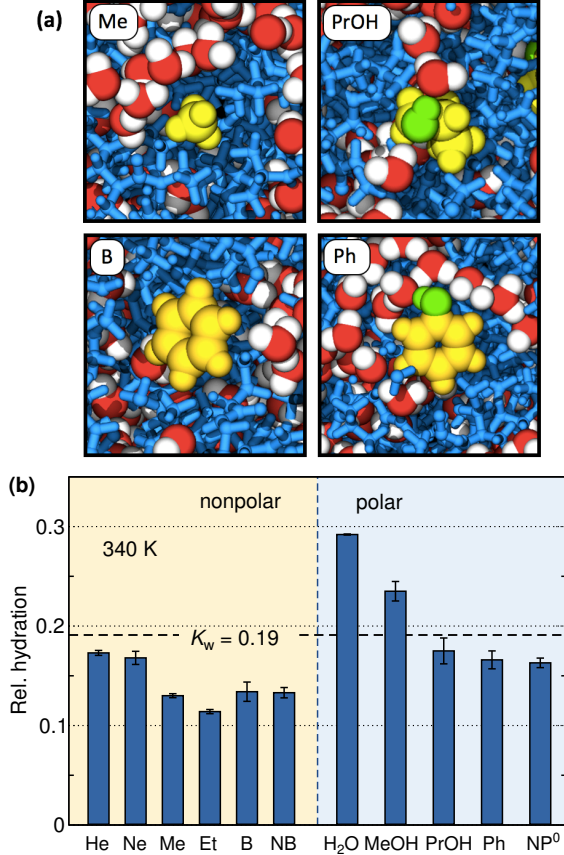


FIG. 3. (a) Cross-section snapshots of Me, PrOH, B, and Ph solutes in PNIPAM phase. For clarity are the hydrophobic parts of the solutes shown in yellow, the hydroxyl groups in green, PNIPAM polymers in blue, and water in red-white. (b) Relative hydration of solutes in the PNIPAM phase at 340 K with respect to bulk water. The water partition ratio in PNIPAM, $K_w = 0.19$ (eq 2) is indicated by a dashed horizontal line and serves as an orientation for the preferred partitioning between water clusters and dry regions of the polymer.

and collapsed PNIPAM phase (G_p), are plotted in Figure 4a.

Universally, the free energies of nonpolar solutes in water are positive, $G_w > 0$, which indicates their low solubility in water. A comparison of the G_w values with experiments shows reasonable agreement (see *Supporting Information*), which validates the combination of the used force fields for our needs. The polar solutes, on the other hand, exhibit significantly negative solvation free energies in water, $G_w < 0$, due to the expected formation of hydrogen bonds between the hydroxyl group and water.

The solvation free energies in PNIPAM, G_p , are

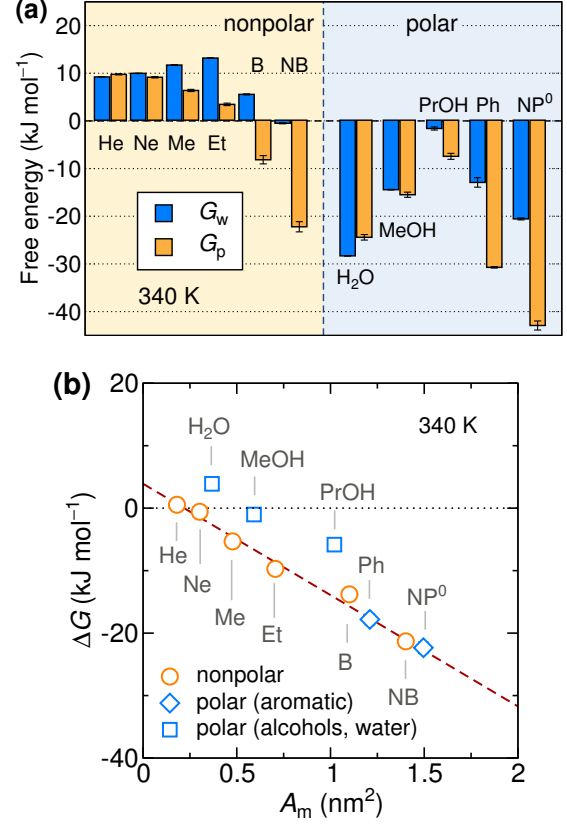


FIG. 4. (a) Solvation free energies of solutes in water G_w (blue) and in PNIPAM G_p (orange) at 340 K. (b) Transfer free energies from water to PNIPAM, $\Delta G = G_p - G_w$, plotted as a function of the molecular surface area. The dashed line is a fit of eq 4 to the data points of nonpolar solutes.

shown in the same plot by orange bars. They are positive and comparable to G_w for small nonpolar molecules, whereas for larger nonpolar as well as for polar molecules, G_p values become negative. A glance at Figure 4a suggests considerable specificity of the interactions, without a simple rule that can be deduced only by looking at the solutes' molecular structure. Clearly, the free energies reflect the complexity of detailed chemical structures.

In the remaining part of the paper we turn our attention to the *transfer* free energies, that is, the difference between the solvation free energies in PNIPAM and in water,

$$\Delta G = G_p - G_w \quad (3)$$

This quantity thus corresponds to the work needed to transfer a solute from bulk water into the PNIPAM phase, and is related to the partition ratio in

the limit of infinite dilution as $K = \exp(-\Delta G/k_B T)$. See also the in-depth discussion on K later on. Figure 4b shows ΔG versus the molecular surface area A_m (see Methods section for the definition of A_m) of the solutes, which reveals a clear linear dependence for the nonpolar solutes. A linear scaling is well known for the hydration free energies of large hydrophobes in bulk water. However, the linearity in our heterogeneous polymer–water medium is surprising. The results can be conveniently described in terms of an effective *molecular surface tension*, γ_m [67, 68],

$$\Delta G = \Delta G_0 + \gamma_m A_m \quad (4)$$

Note that γ_m is not equivalent to the free energy of creating a flat macroscopic interface, and can therefore also be negative. The fit of eq 4 to the nonpolar solutes (dashed line in Figure 4b) gives the value $\gamma_m = -18(1) \text{ kJ mol}^{-1} \text{ nm}^{-2}$. This value of course depends on the definition of the surface area, but the linear dependence (eq 4), as it turns out, is a quite robust feature against the size definition (see *Supporting Information* for the sensitivity of γ_m on the definition of the surface area). Furthermore, the parameter ΔG_0 , which also depends on the choice of the solute size, represents an offset in the linear dependence and does hence not contain a significant physical information.

Turning now to the polar molecules, we notice that both alcohols and water exhibit transfer free energies that are by about 7 kJ/mol above the trend of the nonpolar solutes. This is in line with experimental observations that hydrophobic dyes tend to partition more in PNIPAM-like networks than hydrophilic ones [26]. But, on the other hand, both polar aromatic molecules (Ph and NP⁰) behave very similarly to the nonpolar solutes instead. Namely hydroxyl groups in aromatic molecules have slightly different character than in alkyl chains, owing to the mesomeric and inductive effects of the phenyl group [69]. The phenyl group allows non-bonding electrons on the oxygen to partially delocalize into the ring via π bonding, thus decreasing the electron density in the O–H bond. These small specific effects in the hydroxyl groups thus cause that the polar aromatic solutes behave more alike to the nonpolar ones rather than to polar alkyl molecules (*i.e.*, alcohols). It is somehow remarkable that also the water molecule (*i.e.*, the solvent), perfectly fits the linear scheme of alcohols. Of course, the transfer free energy of a water molecule, which is $\Delta G = 3.9 \text{ kJ/mol}$, represents the excess free energy for transferring a water molecule from bulk into an already fully hydrated PNIPAM. It should therefore not be confused

with the entire free energy of the system, which apart from the excess part contains also the ideal-gas contribution.

D. Partitioning and temperature effects.

When heating or cooling a collapsed PNIPAM, the water content inside adjusts such that it stays in chemical equilibrium with bulk water (cf. Figure 1c). Temperature-dependent transfer free energies ΔG are shown in Figure 5a for several solutes. Small nonpolar solutes (not NB) show an enhanced solubility (decrease in ΔG) in PNIPAM upon heating. On the other hand, all polar molecules exhibit a weakening of solvation (increase in ΔG) upon heating. We will return to the explanation of these results later on.

A central quantity of nanocarrier systems in general is the gel–water partition ratio K , defined as the ratio of the equilibrium concentration in the gel to that in the solution, $K = c^{(\text{in})}/c^{(\text{out})}$, and is in the limit of infinite dilution directly related to the transfer free energy ΔG as

$$K = \exp\left(-\frac{\Delta G}{k_B T}\right) \quad (5)$$

Figure 5b shows partition ratios that follow from the calculated ΔG (shown in panel a). The linear scaling of the transfer free energy with the effective solute surface area (eq 4) thus results in an almost five-orders-of-magnitude wide span of the partition ratios. Water and methanol feature $K \sim 0.1$ –1, small nonpolar molecules (Me, Et) exhibit $K \sim 10^2$, whereas the partitioning of the largest molecules (NB and NP⁰) reaches $K \sim 10^4$.

As opposed to mixed temperature dependencies of ΔG with temperature, K decreases with temperature for all the shown solutes, owing to the additional $1/T$ factor in the exponent of eq 5. In fact, the temperature dependence of ΔG is related to the transfer entropy ΔS ,

$$\left(\frac{\partial \Delta G}{\partial T}\right)_p = -\Delta S \quad (6)$$

On the other hand, the temperature dependence of K is associated with the transfer enthalpy ΔH via the well-known van ’t Hoff equation,

$$\frac{\partial \ln K}{\partial T} = \frac{\Delta H}{k_B T^2} \quad (7)$$

The decrease of K with temperature in our simulations thus indicates exothermic solvation ($\Delta H < 0$) in the PNIPAM phase.

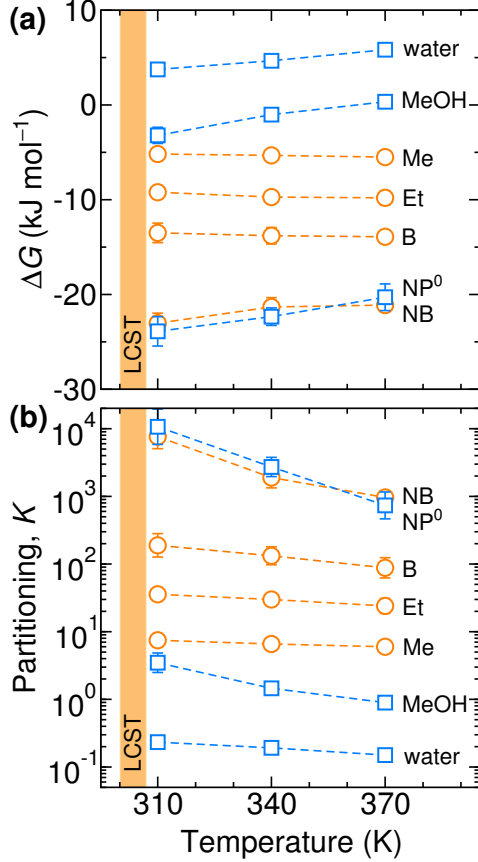


FIG. 5. (a) Transfer free energies ΔG of several solutes as a function of temperature. (b) The PNIPAM–water partition ratio K (computed via eq 5) of the solutes from (a) as a function of temperature. Water content in PNIPAM corresponds to the equilibrium value with bulk water reservoir at each temperature (cf. Figure 1c).

Using eqs 7 and 6, we evaluate the transfer enthalpies and entropies, respectively, which are plotted in Figure 6. The enthalpies are negative, except for the smallest solutes (He and Ne), as already implied from the negative trends of K vs. T in Figure 5b. Interestingly, they scale roughly linearly with the particle surface area, and can be fitted to the relation

$$\Delta H = \Delta H_0 + h_m A_m \quad (8)$$

The proportionality factor h_m here denotes (in analogy to eq 4) the *surface enthalpy*. A fit to the nonpolar solutes (orange dashed line) yields $h_m = -25(5) \text{ kJ mol}^{-1} \text{ nm}^{-2}$. The polar solutes lie consistently below the nonpolar ones by around -10 kJ/mol (as indicated by the blue dashed line

with the same h_m as for the nonpolar solutes).

The entropic contribution (Figure 6b) for small nonpolar solutes (apart from NB) is small, slightly negative and almost independent of the size. This can be partially explained in terms of the unfavorable transfer entropy of small hydrophobes into water [68]. When a solute is transferred from water to more hydrophobic PNIPAM, this results into a weak but favorable free energy component. However, the entropy being so small in magnitude and independent of size is remarkable. We believe also that water molecules with non-saturated hydrogen bonds removed from hydrophobic cavities inside the polymer upon insertion contribute significantly to the free energy, in particular with favorable enthalpy and unfavorable entropy contributions [70, 71]. This enthalpy-driven hydrophobic solvation can also be envisioned as a complementary association of apolar (concave) pocket–(convex) ligand binding, whose thermodynamic signature hardly depends on the particular pocket/ligand geometry [72].

For polar solutes, on the other hand, the unfavorable entropy may be related to their restricted (especially rotational) degrees of freedom in the PNIPAM phase. The hydrogen bonds formed between a solute, either with sorbed water or with polymer chains, act as anchors to their motion. In this respect, also a large NB (although classified as nonpolar) can actually form hydrogen bonds via the NO_2 group and thus its transfer entropy is in the midway between other nonpolar solutes and the polar ones.

E. Adsorption on an elongated chain. The atomistic model utilized in this study serves us to obtain an insight into the solvation in a collapsed hydrogel, above the volume transition temperature. Below the transition temperature, a cross-linked PNIPAM hydrogel swells and increases the amount of water typically by an order of magnitude, such that neighboring chains tend to move significantly far apart. A simple model system of a swollen gel was investigated by us in a previous study [40], where we assessed adsorption properties of solutes on a single elongated PNIPAM chain (a snapshot shown in Figure 7a). It is now interesting to compare solvation in the collapsed and the swollen states of PNIPAM.

The total particle adsorption ΔN on a single chain is proportional to the bulk concentration of the solutes, $c^{(\text{out})}$, as $\Delta N = \Gamma' L_z c^{(\text{out})}$, where L_z is the projected chain length and Γ' stands for the adsorption coefficient [40]. Note that Γ' depends on the chain elongation λ (not to be confused with the coupling pa-

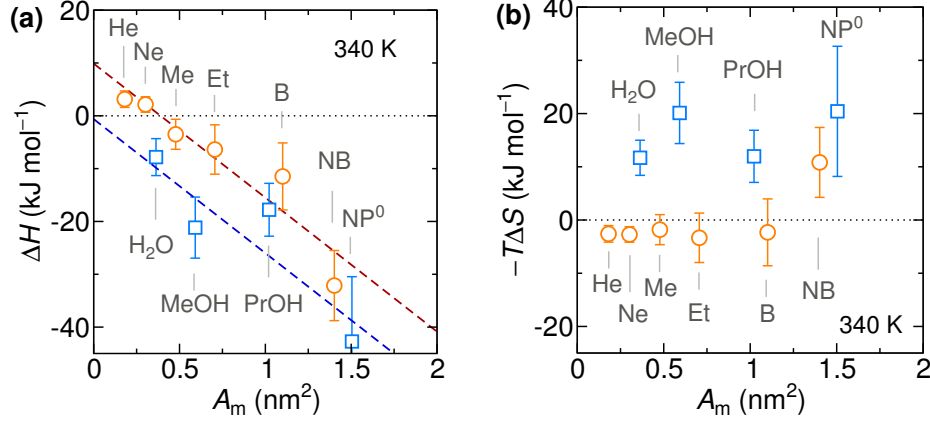


FIG. 6. Decomposition of the transfer free energy ΔG into (a) the enthalpic and (b) entropic contributions at 340 K.

parameter in TI), defined as the ratio of the projected chain length and the contour length L_c of the chain, $\lambda = L_z/L_c$. The adsorption free energy for this system is subject to the definition of bound and unbound states. In a simplified picture (Figure 7b), we can approximate the concentration of the adsorbed solutes in the vicinity of the chain by assuming an effective radius of the chain, $R_0 = 0.5$ nm (determined as the Gibbs dividing surface of water [40]), and specifying an effective adsorption region around the chain cylinder with the width of a typical solute size, $\delta = 0.25$ nm. With that, the concentration of adsorbed solutes expresses as $c_{\text{ads}} = \Delta N/(2\pi R_0 \delta L_z)$. The adsorption free energy on a single chain can then be computed as $G_{\text{ads}} = -k_B T \ln(c_{\text{ads}}/c^{(\text{out})})$, which can be written in terms of the adsorption coefficient Γ' as

$$G_{\text{ads}} = k_B T \ln(2\pi R_0 \delta) - k_B T \ln \Gamma' \quad (9)$$

Here, the geometrical continuum-model parameters R_0 and δ contribute only to a shift (first term) of the free energy, whereas all essential adsorption information is incorporated in the second term.

In Figure 7c we compare the transfer free energies ΔG in the collapsed PNIPAM (empty symbols) from this study with the adsorption free energies G_{ads} on a single chain (full symbols) obtained from Γ' for the elongation $\lambda = 0.83$ (Ref. [40]) using eq 9. As can be seen, similarly to ΔG , also G_{ads} scales approximately linearly with the surface area of the solute, albeit with a different slope. A linear fit of eq 4 to the nonpolar data points for G_{ads} gives the value $\gamma_m^{(\text{ads})} = -9(2)$ kJ mol $^{-1}$ nm $^{-2}$. That is, the molecular surface tension of the adsorption on a single chain is roughly half the value of the

transfer of nonpolar solutes into the collapsed state ($\gamma_m = -18(1)$ kJ mol $^{-1}$ nm $^{-2}$). Neglecting the offsets of the fits, we can deduce an empirical relation

$$G_{\text{ads}} \approx \Delta G/2 \quad (10)$$

Its simple interpretation can be that as a solute adsorbs on a single chain it exposes only a half of its surface to the chain, whereas the other half faces the water phase. It is also interesting that the adsorption free energies are almost insensitive to the polarity of the solutes: As has been shown [40], a polar solute that adsorbs on the chain points its OH group away from the chain, thus making it less relevant for the adsorption. In contrast, if the solute solvates inside the collapsed PNIPAM phase, the OH group has to be accommodated within other polymer chains, making its contribution much more significant.

Note that the PNIPAM models differ a bit in the two studies. PNIPAM chains in Ref. [40] are isotactic, whereas they are atactic in this study. As has been shown [40], the adsorption varies by less than 25% among different tacticities, which yields only around 1 kJ/mol variance in the adsorption free energy (eq 9). The other difference is that the force field for PNIPAM in Ref. [40] is the standard OPLS-AA [50], which slightly differs in partial charges from the one used in this study, yet we believe that this should not alter our qualitative conclusions.

F. Partitioning: Swollen vs. collapsed state.

We now make a step further and use the observation given by eq 10 to relate the partition ratios in the swollen and collapsed state of a hydrogel. Assuming that the gel in the swollen state is very dilute, such

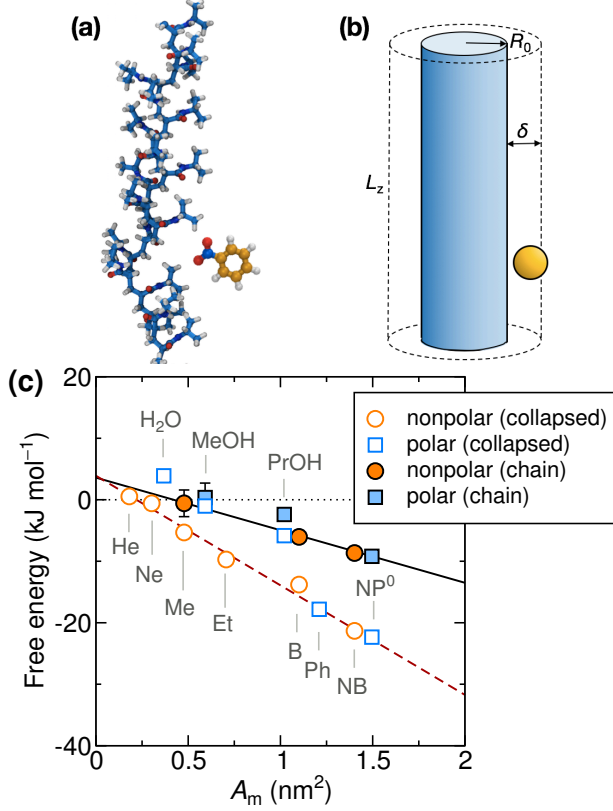


FIG. 7. (a) Snapshot of a single elongated PNIPAM chain with a nitrobenzene molecule about to adsorb. (b) Continuum representation of the chain with radius R_0 and an adsorbing region of a thickness δ . (c) Comparison of relative solvation free energies in a collapsed PNIPAM (same as in Figure 4b) and the adsorption energies on a single PNIPAM chain evaluated from Ref. [40] via eq 9. The lines are fits of eq 4 to the data points of nonpolar solutes.

that adjacent polymer chains are elongated and far apart, and that the effects of cross-linkers can be ignored, we can calculate the total number of solutes inside the gel, N_{in} , from the adsorption on all its chains,

$$N_{\text{in}} = c^{(\text{out})}V + \Gamma' \lambda L_c c^{(\text{out})} \quad (11)$$

The first term corresponds to the non-adsorbed solute background in the gel and the second term is the number of adsorbed solutes on all the chains with a total contour length L_c . Using eq 9 and expressing the contour length in terms of the polymer volume fraction, $\phi_p = \pi R_0^2 L_c / V$, we arrive at the following expression for the partition ratio in the swollen state

$$K^{(s)} = 1 + \phi_p (2\lambda\delta / R_0) e^{-G_{\text{ads}} / k_B T} \quad (12)$$

Evaluating the numerical factor $2\lambda\delta / R_0 \simeq 1$ (note that $\lambda \approx 0.8$ is close to unity for a very swollen gel) and using eq 10 together with eq 5, we finally obtain the relation between the partition ratios for nonpolar solutes in the collapsed (K) and swollen ($K^{(s)}$) states

$$K^{(s)} \simeq 1 + \phi_p^{(s)} \sqrt{K} \quad (13)$$

In our model of the collapsed state of a PNIPAM gel, the partition ratio for larger aromatic molecules is $K \sim 10^3$ – 10^4 (Figure 5b). Now, assuming a typical polymer volume fraction of $\phi_p = 0.1$ in the swollen state, the above equation gives the the partition ratio in the swollen state of only $K^{(s)} \simeq 4$ – 10 , which we also obtained in our previous work [40]. This simple relation demonstrates an enormous impact that a changing environment from hydrophilic (swollen state) to hydrophobic (collapsed state) has on the partitioning. Namely, doubling the hydrophobic interaction in the collapsed state as suggested by eq 10, results in a quadratic relation of the partition ratios, $K \propto K^{(s)2}$.

On the other hand, polar solutes are subject to more specific interactions, such that we cannot design a similar simple rule. We found for instance that polar aromatic molecules follow similar trend as nonpolar molecules, thus eq 13 is applicable for them as well. On the other hand, for the two alcohols one can rather consider $G_{\text{ads}} \approx \Delta G$, which results in a linear scaling of both partition ratios, namely $K^{(s)} \simeq 1 + \phi_p^{(s)} K$.

IV. CONCLUSIONS

We have performed extensive all-atom molecular dynamics simulations of solvation of small subnanometer-sized solutes in collapsed PNIPAM polymers in equilibrium with water. Sorbed and heterogeneously distributed water between the polymer chains, whose content depends on temperature, causes non-uniform partitioning of the solutes. Nonpolar solutes are preferentially expelled from water clusters and tend to reside in ‘dryer’ regions of the gel, whereas polar molecules tend to partition closer to or in water clusters.

The transfer free energy from water into PNIPAM of nonpolar solutes scales very well with an effective molecular surface area, thus making it the decisive descriptor. The presence of a hydroxyl group in generally opposes the solvation in PNIPAM, but its nature is not as deterministic as the surface area, especially for aromatic molecules. The partition ratios

of the studied small solute molecules, spanning from neon to benzene derivatives, span over five orders in magnitude.

Finally, an important observation that we find is a strong correlation between the transfer free energies into a collapsed PNIPAM and the adsorption free energies to a single PNIPAM chain. The adsorption free energies are about one half the values of the transfer free energies. This can be explained in a sense that an adsorbed solute exposes only a half of its surface to the polymer chain and the other half faces the water phase, whereas a solvated solute exposes its entire surface area to the PNIPAM phase. As a consequence, the partition ratio in the collapsed state scales quadratically with the partition ratio in the swollen state. That means that the release/uptake of the gel undergoing a swelling/collapse is particularly large for larger nonpolar molecules.

Understanding the solvation mechanisms inside not only PNIPAM but also other responsive hydrogels is important for the rational design of novel materials. The next important step in understanding these systems would be to analyze the solvation properties of

ions and the effects of cross-linkers in these gel models, which are our future objectives.

Conflict of Interest. The authors declare no competing financial interest.

Supporting Information Description. Solvation in water: MD vs. experiments; Solute-solute contribution; Sensitivity to the effective solute surface area

Acknowledgments. The authors thank Yan Lu and Matthias Ballauff for useful discussions. This project has received funding from the European Research Council (ERC) under the European Union's Horizon 2020 research and innovation programme (Grant Agreement No. 646659-NANOREACTOR). M.K. acknowledges the financial support from the Slovenian Research Agency (research core funding no. P1-0055). The simulations were performed with resources provided by the North-German Supercomputing Alliance (HLRN).

-
- [1] Klouda, L.; Mikos, A. G. Thermoresponsive Hydrogels in Biomedical Applications. *Eur. J. Pharm. Biopharm.* **2008**, *68*, 34–45.
 - [2] Peppas, N. A. Hydrogels and Drug Delivery. *Curr. Opin. Colloid Interface Sci.* **1997**, *2*, 531–537.
 - [3] Stuart, M. A. C.; Huck, W. T.; Genzer, J.; Muller, M.; Ober, C.; Stamm, M.; Sukhorukov, G. B.; Szleifer, I.; Tsukruk, V. V.; Urban, M.; et al., Emerging Applications of Stimuli-responsive Polymer Materials. *Nat. Mater.* **2010**, *9*, 101–113.
 - [4] Kabanov, A.; Vinogradov, S. Nanogels as Pharmaceutical Carriers: Finite Networks of Infinite Capabilities. *Angew. Chem. Int.* **2009**, *48*, 5418–5429.
 - [5] Oh, J. K.; Drumright, R.; Siegwart, D. J.; Matyjaszewski, K. The Development of Microgels/Nanogels for Drug Delivery Applications. *Prog. Polym. Sci.* **2008**, *33*, 448–477.
 - [6] Guan, Y.; Zhang, Y. PNIPAM Microgels for Biomedical Applications: From Dispersed Particles to 3D Assemblies. *Soft Matter* **2011**, *7*, 6375–6384.
 - [7] Zhang, J.-T.; Wei, G.; Keller, T. F.; Gallagher, H.; Stötz, C.; Müller, F. A.; Gottschaldt, M.; Schubert, U. S.; Jandt, K. D. Responsive Hybrid Polymeric/Metallic Nanoparticles for Catalytic Applications. *Macromol. Mater. Eng.* **2010**, *295*, 1049–1057.
 - [8] Lu, Y.; Proch, S.; Schrunner, M.; Drechsler, M.; Kempe, R.; Ballauff, M. Thermosensitive Core-Shell Microgel as a "Nanoreactor" for Catalytic Active Metal Nanoparticles. *J. Mater. Chem.* **2009**, *19*, 3955–3961.
 - [9] Wu, S.; Dzubiella, J.; Kaiser, J.; Drechsler, M.; Guo, X.; Ballauff, M.; Lu, Y. Thermosensitive Au-PNIPAM Yolk-Shell Nanoparticles with Tunable Selectivity for Catalysis. *Angew. Chem. Int.* **2012**, *51*, 2229–2233.
 - [10] Lapeyre, V.; Gosse, I.; Chevreux, S.; Ravaine, V. Monodispersed Glucose-Responsive Microgels Operating at Physiological Salinity. *Biomacromolecules* **2006**, *7*, 3356–3363.
 - [11] Parasuraman, D.; Serpe, M. J. Poly (N-Isopropylacrylamide) Microgel-Based Assemblies for Organic Dye Removal from Water. *ACS Appl. Mater. Interfaces* **2011**, *3*, 4714–4721.
 - [12] Nykänen, A.; Nuopponen, M.; Laukkanen, A.; Hirvonen, S.-P.; Rytelä, M.; Turunen, O.; Tenhu, H.; Mezzenga, R.; Ikkala, O.; Ruokolainen, J. Phase Behavior and Temperature-Responsive Molecular Filters Based on Self-Assembly of Polystyrene-block-poly (N-isopropylacrylamide)-block k-polystyrene. *Macromolecules* **2007**, *40*, 5827–5834.
 - [13] Chen, J.; Ahmad, A.; Ooi, B. Thermo-Responsive Properties of Poly (N-isopropylacrylamide-co-

- acrylic Acid) Hydrogel and Its Effect on Copper Ion Removal and Fouling of Polymer-Enhanced Ultrafiltration. *J. Membr. Sci.* **2014**, *469*, 73–79.
- [14] Hyk, W.; Kitka, K. Water Purification Using Sponge Like Behaviour of Poly (N-isopropylacrylamide) Ferrogels. Studies on Silver Removal from Water Samples. *J. Environ. Chem. Eng.* **2018**, *6*, 6108–6117.
- [15] Pelton, R. Temperature-Sensitive Aqueous Microgels. *Adv. Colloid Interface Sci.* **2000**, *85*, 1–33.
- [16] Gil, E. S.; Hudson, S. M. Stimuli-Reponsive Polymers and their Bioconjugates. *Prog. Polym. Sci.* **2004**, *29*, 1173–1222.
- [17] Halperin, A.; Kröger, M.; Winnik, F. M. Poly (N-isopropylacrylamide) Phase Diagrams: Fifty Years of Research. *Angew. Chem. Int. Ed.* **2015**, *54*, 15342–15367.
- [18] Lu, Y.; Mei, Y.; Drechsler, M.; Ballauff, M. Thermosensitive Core-Shell Particles as Carriers for Ag Nanoparticles: Modulating the Catalytic Activity by a Phase Transition in Networks. *Angew. Chem. Int.* **2006**, *45*, 813–816.
- [19] Ballauff, M.; Lu, Y. ‘Smart’ Nanoparticles: Preparation, Characterization and Applications. *Polymer* **2007**, *48*, 1815–1823.
- [20] Leo, A.; Hansch, C.; Elkins, D. Partition Coefficients and Their Uses. *Chem. Rev.* **1971**, *71*, 525–616.
- [21] McNaught, A. D.; Wilkinson, A. *IUPAC. Compendium of Chemical Terminology, 2nd ed. (the “Gold Book”)*; Blackwell Scientific Publications, Oxford, 1997.
- [22] Chiou, C. T.; Schmedding, D. W.; Manes, M. Improved Prediction of Octanol–Water Partition Coefficients from Liquid–Solute Water Solubilities and Molar Volumes. *J. Environ. Sci. Technol.* **2005**, *39*, 8840–8846.
- [23] Roa, R.; Kim, W. K.; Kanduč, M.; Dzubiella, J.; Angioletti-Uberti, S. Catalyzed Bimolecular Reactions in Responsive Nanoreactors. *ACS Catal.* **2017**, *7*, 5604–5611.
- [24] Merrill, E. W.; Dennison, K. A.; Sung, C. Partitioning and Diffusion of Solutes in Hydrogels of Poly(Ethylene Oxide). *Biomaterials* **1993**, *14*, 1117–1126.
- [25] Palasis, M.; Gehrke, S. H. Permeability of Responsive Poly(N-isopropylacrylamide) Gel to Solutes. *J. Control Release.* **1992**, *18*, 1–11.
- [26] Guilherme, M.; Silva, R.; Girotto, E.; Rubira, A.; Muniz, E. Hydrogels Based on PAAm Network with PNIPAAm Included: Hydrophilic–Hydrophobic Transition Measured by the Partition of Orange II and Methylene Blue in Water. *Polymer* **2003**, *44*, 4213–4219.
- [27] Molina, M.; Rivarola, C.; Barbero, C. Study on Partition and Release of Molecules in Superabsorbent Thermosensitive Nanocomposites. *Polymer* **2012**, *53*, 445–453.
- [28] Katritzky, A. R.; Maran, U.; Lobanov, V. S.; Karelson, M. Structurally Diverse Quantitative Structure-Property Relationship Correlations of Technologically Relevant Physical Properties. *J. Chem. Inf. Comput. Sci.* **2000**, *40*, 1–18.
- [29] Duffy, E. M.; Jorgensen, W. L. Prediction of Properties from Simulations: Free Energies of Solvation in Hexadecane, Octanol, and Water. *J. Am. Chem. Soc.* **2000**, *122*, 2878–2888.
- [30] Jorgensen, W. L.; Duffy, E. M. Prediction of Drug Solubility from Structure. *Adv. Drug Deliv. Rev.* **2002**, *54*, 355–366.
- [31] Aydt, E.; Hentschke, R. Swelling of a Model Network: A Gibbs-Ensemble Molecular Dynamics Study. *J. Chem. Phys.* **2000**, *112*, 5480–5487.
- [32] Erbas, A.; Olvera de la Cruz, M. Energy Conversion in Polyelectrolyte Hydrogels. *ACS Macro Lett.* **2015**, *4*, 857–861.
- [33] Košovan, P.; Richter, T.; Holm, C. Modeling of Polyelectrolyte Gels in Equilibrium with Salt Solutions. *Macromolecules* **2015**, *48*, 7698–7708.
- [34] Kim, W. K.; Moncho-Jordá, A.; Roa, R.; Kanduč, M.; Dzubiella, J. Cosolute Partitioning in Polymer Networks: Effects of Flexibility and Volume transitions. *Macromolecules* **2017**, *50*, 6227–6237.
- [35] Pérez-Mas, L.; Martín-Molina, A.; Quesada-Pérez, M.; Moncho-Jordá, A. Maximizing the Absorption of Small Cosolutes Inside Neutral Hydrogels: Steric Exclusion Versus Hydrophobic Adhesion. *Phys. Chem. Chem. Phys.* **2018**, *20*, 2814–2825.
- [36] Quesada-Pérez, M.; Maroto-Centeno, J. A.; Martín-Molina, A.; Moncho-Jordá, A. Direct Determination of Forces between Charged Nanogels through Coarse-Grained Simulations. *Phys. Rev. E* **2018**, *97*, 042608.
- [37] Rodríguez-Ropero, F.; van der Vegt, N. F. Direct Osmolyte–Macromolecule Interactions Confer Entropic Stability to Folded States. *J. Phys. Chem. B* **2014**, *118*, 7327–7334.
- [38] Rodríguez-Ropero, F.; van der Vegt, N. F. A. On the Urea Induced Hydrophobic Collapse of a Water Soluble Polymer. *Phys. Chem. Chem. Phys.* **2015**, *17*, 8491–8498.
- [39] Pérez-Fuentes, L.; Drummond, C.; Faraudo, J.; Bastos-González, D. Anions Make the Difference: Insights from the Interaction of Big Cations and Anions with Poly (N-isopropylacrylamide) Chains and Microgels. *Soft Matter* **2015**, *11*, 5077–5086.
- [40] Kanduč, M.; Chudoba, R.; Palczynski, K.; Kim, W. K.; Roa, R.; Dzubiella, J. Selective Solute Adsorption and Partitioning around Single PNIPAAm Chains. *Phys. Chem. Chem. Phys.* **2017**, *19*, 5906–5916.
- [41] Kanduč, M.; Kim, W. K.; Roa, R.; Dzubiella, J. Selective Molecular Transport in Thermo-responsive Polymer Membranes: Role of Nanoscale Hydration and Fluctuations. *Macromolecules* **2018**, *51*, 4853–

- 4864.
- [42] Palivec, V.; Zadrazil, D.; Heyda, J. All-Atom REMD Simulation of Poly-N-isopropylacrylamide Thermodynamics in Water: a Model with a Distinct 2-State Behavior. *arXiv preprint arXiv:1806.05592* **2018**,
 - [43] Walter, J.; Ermatchkov, V.; Vrabec, J.; Hasse, H. Molecular Dynamics and Experimental Study of Conformation Change of Poly(N-isopropylacrylamide) Hydrogels in Water. *Fluid Phase Equilib.* **2010**, *296*, 164–172.
 - [44] Algaer, E. A.; van der Vegt, N. F. A. Hofmeister Ion Interactions with Model Amide Compounds. *J. Phys. Chem. B* **2011**, *115*, 13781–13787.
 - [45] Tucker, A. K.; Stevens, M. J. Study of the Polymer Length Dependence of the Single Chain Transition Temperature in Syndiotactic Poly(N-isopropylacrylamide) Oligomers in Water. *Macromolecules* **2012**, *45*, 6697–6703.
 - [46] Mukherji, D.; Kremer, K. Coil–Globule–Coil Transition of Nipam in Aqueous Methanol: Coupling All-Atom Simulations to Semi-Grand Canonical Coarse-Grained Reservoir. *Macromolecules* **2013**, *46*, 9158–9163.
 - [47] Chiessi, E.; Paradossi, G. Influence of Tacticity on Hydrophobicity of Poly (N-isopropylacrylamide): A Single Chain Molecular Dynamics Simulation Study. *J. Phys. Chem. B* **2016**, *120*, 3765–3776.
 - [48] Adroher-Benítez, I.; Moncho-Jordá, A.; Odríozola, G. Conformation Change of an Isotactic Poly (N-isopropylacrylamide) Membrane: Molecular Dynamics. *J. Chem. Phys.* **2017**, *146*, 194905.
 - [49] Berendsen, H. J. C.; Grigera, J. R.; Straatsma, T. P. The Missing Term in Effective Pair Potentials. *J. Phys. Chem.* **1987**, *91*, 6269–6271.
 - [50] Jorgensen, W. L.; Tirado-Rives, J. The OPLS [Optimized Potentials for Liquid Simulations] Potential Functions for Proteins, Energy Minimizations for Crystals of Cyclic Peptides and Crambin. *J. Am. Chem. Soc.* **1988**, *110*, 1657–1666.
 - [51] Price, M. L. P.; Ostrovsky, D.; Jorgensen, W. L. Gas-Phase and Liquid-State Properties of Esters, Nitriles, and Nitro Compounds with the OPLS-AA Force Field. *J. Comp. Chem.* **2001**, *22*, 1340–1352.
 - [52] Hess, B.; van der Vegt, N. F. Hydration Thermodynamic Properties of Amino Acid Analogues: A Systematic Comparison of Biomolecular Force Fields and Water Models. *J. Phys. Chem. B* **2006**, *110*, 17616–17626.
 - [53] Van Durme, K.; Van Assche, G.; Van Mele, B. Kinetics of Demixing and Remixing in Poly (N-isopropylacrylamide)/Water Studied by Modulated Temperature DSC. *Macromolecules* **2004**, *37*, 9596–9605.
 - [54] Dong, L.-C.; Hoffman, A. S. Synthesis and Application of Thermally Reversible Heterogels for Drug Delivery. *J. Control. Release* **1990**, *13*, 21–31.
 - [55] Sasaki, S.; Koga, S.; Maeda, H. Dielectric Properties of Collapsing Hydrogels. *Macromolecules* **1999**, *32*, 4619–4624.
 - [56] van der Spoel, D.; Lindahl, E.; Hess, B.; Groenhof, G.; Mark, A. E.; Berendsen, H. J. C. GROMACS: Fast, Flexible, and Free. *J. Comput. Chem.* **2005**, *26*, 1701–1718.
 - [57] Pronk, S.; Páll, S.; Schulz, R.; Larsson, P.; Bjelkmar, P.; Apostolov, R.; Shirts, M. R.; Smith, J. C.; Kasson, P. M.; van der Spoel, D.; Hess, B.; Lindahl, E. GROMACS 4.5: A High-Throughput and Highly Parallel Open Source Molecular Simulation Toolkit. *Bioinformatics* **2013**, *29*, 845–854.
 - [58] Berendsen, H. J. C.; Postma, J. P. M.; van Gunsteren, W. F.; DiNola, A.; Haak, J. R. Molecular Dynamics with Coupling to an External Bath. *J. Chem. Phys.* **1984**, *81*, 3684–3690.
 - [59] Bussi, G.; Donadio, D.; Parrinello, M. Canonical Sampling through Velocity Rescaling. *J. Chem. Phys.* **2007**, *126*.
 - [60] Darden, T.; York, D.; Pedersen, L. Particle mesh Ewald: An $N \log(N)$ Method for Ewald Sums in Large Systems. *J. Chem. Phys.* **1993**, *98*, 10089–10092.
 - [61] Essmann, U.; Perera, L.; Berkowitz, M. L.; Darden, T.; Lee, H.; Pedersen, L. G. A Smooth Particle Mesh Ewald Method. *J. Chem. Phys.* **1995**, *103*, 8577–8593.
 - [62] Frenkel, D.; Ladd, A. J. New Monte Carlo Method to Compute the Free Energy of Arbitrary Solids. Application to the FCC and HCP Phases of Hard Spheres. *J. Chem. Phys.* **1984**, *81*, 3188–3193.
 - [63] Beutler, T. C.; Mark, A. E.; van Schaik, R. C.; Gerber, P. R.; van Gunsteren, W. F. Avoiding Singularities and Numerical Instabilities in Free Energy Calculations Based on Molecular Simulations. *Chem. Phys. Lett.* **1994**, *222*, 529–539.
 - [64] Karelson, M. *Molecular Descriptors in QSAR/QSPR*; Wiley-Interscience, 2000.
 - [65] Shrake, A.; Rupley, J. Environment and Exposure to Solvent of Protein Atoms. Lysozyme and Insulin. *Biochem. Mol. Biol. J.* **1973**, *79*, 351–371.
 - [66] Eisenhaber, F.; Lijnzaad, P.; Argos, P.; Sander, C.; Scharf, M. The Double Cubic Lattice Method: Efficient Approaches to Numerical Integration of Surface Area and Volume and to Dot Surface Contouring of Molecular Assemblies. *J. Comput. Chem.* **1995**, *16*, 273–284.
 - [67] Tanford, C. Interfacial Free Energy and the Hydrophobic Effect. *Proc. Natl. Acad. Sci.* **1979**, *76*, 4175–4176.
 - [68] Ashbaugh, H. S.; Pratt, L. R. Colloquium: Scaled Particle Theory and the Length Scales of Hydrophobicity. *Rev. Mod. Phys.* **2006**, *78*, 159.
 - [69] Hansch, C.; Leo, A.; Taft, R. A Survey of Hammett Substituent Constants and Resonance and Field Parameters. *Chem. Rev.* **1991**, *91*, 165–195.
 - [70] Setny, P.; Baron, R.; McCammon, J. A. How can Hydrophobic Association be Enthalpy Driven? *J. Chem. Theory Comput* **2010**, *6*, 2866–2871.

- [71] Weiß, R. G.; Setny, P.; Dzubiella, J. Principles for Tuning Hydrophobic Ligand–Receptor Binding Kinetics. *J. Chem. Theory Comput.* **2017**, *13*, 3012–3019.
- [72] Dzubiella, J. How Interface Geometry Dictates Water’s Thermodynamic Signature in Hydrophobic Association. *J. Stat. Phys.* **2011**, *145*, 227–239.